Radboud University Nijmegen

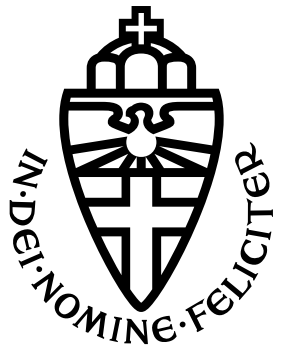

Faculty of Science

Graphene as a particle detector

Thesis BSc Physics and Astronomy

Author:
Simon Peek

Supervisor:
Prof. dr. N. de Groot

Second reader:
Prof. dr. U. Zeitler

July 2022

Abstract

Graphene rocked the world in 2004 when two researchers at the University of Manchester produced the first samples of graphene and discovered its fascinating properties. Since then, graphene has sparked the interest of many research groups. Among them are members of the PTOLEMY project, who aim to measure neutrinos coming from the early stages of the Universe. In this project graphene plays an important role in storing tritium. However, still a lot of research needs to be done on graphene, for instance on the interaction between electrons and graphene. In this thesis graphene will be used in the form of a graphene field effect transistor (GFET) to try and detect a beta particle by measuring a small change in its transfer curve. The first step towards this goal is try and measure a steady transfer curve. This has been done by the use of the so-called *Probe setup*, which gave some promising results corresponding to the data sheet of the GFET. After repeating the measurements the graphene chip eventually stopped working and a second setup, named the *Chip carrier setup*, was constructed. Graphene chips with and without a layer of PMMA on top were used and the measurements were also done before and after annealing. These results showed a steady transfer curve of high quality, especially after annealing the chip. A setup with a silicon photomultiplier operates as comparison tool to the graphene measurements. However, due to the fact that the scintillator emitted photons with a wrong wavelength, the end goal of this project has not yet been reached.

Contents

CHAPTER 1

Introduction

1.1 A new wonder material

Carbon is one of the most versatile, all-round materials on our earth. It literally is the building block for almost all life on our planet. Carbon has four valence electrons which can form chemical bonds in many different ways. This is the main reason that it is a very useful material. Two of the valence electrons are located in s orbitals, while the other two are sitting in p orbitals. Orbital hybridization can take place inside the atom, meaning that one of the electrons in the s orbital is excited to a p orbital. Then one (sp^1-hybridization), two (sp^2-hybridization) or all three (sp^3-hybridization) of the p orbitals mix with the remaining s orbital. Different allotropes of carbon are shown in figure 1.1; zero-dimensional buckyballs, one-dimensional nanotubes, three-dimensional graphite and three dimensional diamond. These different structures have a huge variety of physical properties, but have at least one thing in common; their basing building block, which is a two-dimensional material, is the same. This two-dimensional material literally can be wrapped up into a zero-dimensional buckyball, rolled into a one-dimensional nanotube or stacked into three-dimensional graphite. This allotrope of carbon therefore plays a fundamental roll in understanding the electronic properties in the other allotropes. Although it was known that this material was the literal building block of a variety of different materials, it was presumed to not exist in the free state by theorists for a long time.

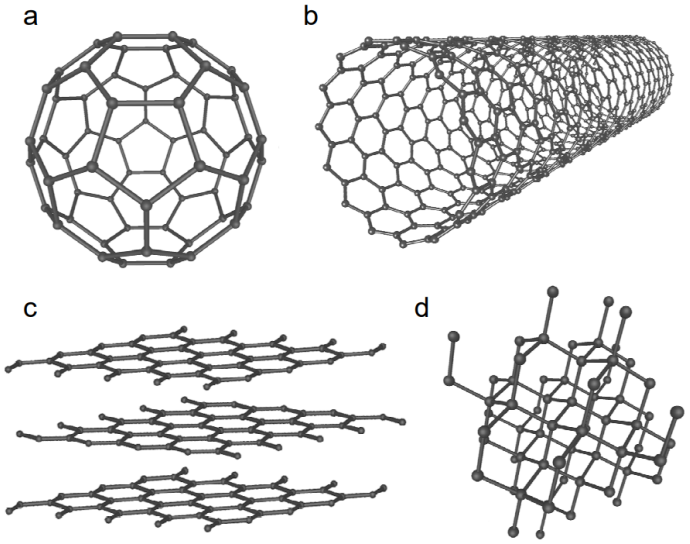

Figure 1.1: Different allotropes of carbon. A few examples are the zero-dimensional buckyballs (a), the one-dimensional nanotubes (b), three-dimensional graphite (c), which consists of a stack of graphene layers and three-dimensional diamond (d) [10].

Nevertheless, a group of researchers from the University of Manchester led by A. K. Geim proved them all wrong when they isolated a single layer of this two-dimensional material [19], [20]. The new material goes under the name of graphene, with its atoms arranged in a two-dimensional hexagonal structure. The method that the research group of Geim developed permitted them to isolate a single layer of the two-dimensional graphene on top of a thick wafer of silicon oxide (SiO_2) with a thickness of 300 nm.The three-dimensional material graphite played a key role in the discovery of graphene. Since it is made out of two-dimensional graphene layers held together by the van der Waals force, researchers searched for a method to peel one layer of graphene out of the graphite. Once on top of the wafer, the weak van der Waals force induces adhesion between the layer of graphene and the silicon oxide wafer. It also creates a very subtle optical effect on top of the silicon layer, which was the reason the single layer of graphene was eventually spotted by an optical microscope. This observation proved the existence of graphene in the physical free state. With its interesting and unique set of thermal, mechanical and electronic properties, it attracted the attention from a broad group of researchers [5].

1.2 The PTOLEMY project

The idea of the Big Bang as the starting point of our Universe fascinates researchers since it was proposed for the first time. If the Universe is constantly expanding, one

could extrapolate back to when it was smaller and less old to eventually reach its starting point. Because of this, there should be a signal left from this early stages that is known as the cosmic neutrino background (CNB). This was theorized a long time ago, but it was assumed to be undetectable nowadays. However, researchers all over the world joined forces and have developed an idea for a design of a CNB detector. The project that aims to develop this detector is called PTOLEMY.
Neutrinos belong to the most elusive particles on earth. They interact with almost nothing and propagate through space unhindered. This together with the fact that they are almost massless and also have no electrical charge makes them very hard to detect. Besides that, during their 13 billion year adventure they cooled down, which means the amount of energy they carry is reduced to a very small amount. Because of the lack of interaction, they do contain a lot of information about their initial stages. The CNB could therefore provide fundamental new information about the first moments after the Big Bang. The idea of the PTOLEMY project is to make use of an unstable naturally occurring isotope of water called tritium (T). This radioactive isotope decays into helium-3 ($^3_2$He) by the emission of an electron e^- and an antineutrino $\bar{\nu}_e$ in the process that can be described by the following decay reaction:

$$^3_1H \longrightarrow {}^3_2He + e^- + \bar{\nu}_e. \tag{1.1}$$

By looking at the exact energy of the emitted electron, one could see if the tritium absorbed a neutrino from the CNB just before it decayed. By absorbing a neutrino, tritium still decays into helium-3, but now only emitting an electron in the process which is given by

$$\nu_e + {}^3_1H \longrightarrow {}^3_2He + e^-. \tag{1.2}$$

This electron would have a slightly bigger energy than an electron emitted by beta decay. The PTOLEMY project aims to measure such a slightly different electron energy and thereby detect a neutrino from the CNB.
The idea of the PTOLEMY project is promising but very challenging with a lot of possible issues on the road. For instance, a question that arises is if the tritium can be kept stable for several years. A gram of tritium produces billions of decay reactions per second, but even then one predicts that there will only be five to ten neutrinos per year detected. Most of the neutrinos still pass through without interacting. The tritium therefore needs to be stable for various years. This could be done by storing the tritium atoms in a two-dimensional layer of graphene. Because of the fact that

graphene is a relatively new material, the proposed PTOLEMY project contains a lot of research that still needs to be done on graphene: check if the material can serve as a target substrate, measure its characteristics when bonding with tritium or hydrogen and take a closer look at the interaction between electrons and graphene [1], [2].

1.3 Graphene as a particle detector

As already stated above, graphene has excellent thermal, mechanical and electronic properties. The thin two-dimensional layer is able to let an ion with low energy pass through without the loss of a huge amount of its kinetic energy. A problem that a lot of contemporary detectors face is the loss of a significant amount of energy of an ion in the detectors, which makes it harder to detect it. It looks like this problem could be eliminated by the use of graphene. Furthermore, the carrier mobility in graphene is very high. Carriers can therefore move quickly through the material, which results in a fast response of graphene to a passing ion. Additionally, the mechanical robustness of graphene prevents the emission of carbon atoms when ions penetrate the material. The thermal mobility of graphene also gives it a significant advantage: it prevents the formation of thermal spikes when an ion penetrates the graphene. Thermal spikes can cause vacancies in the graphene, which lower the quality of the material.
The combination of these properties makes graphene a great candidate for a particle detector. There has already been done research on the utility of graphene as an alpha particle detector [16] and as an neutral particle detector [24] as well. In this thesis graphene will be used to try and detect a beta particle, something on which a lot less research has been done until today [1].

CHAPTER 2

Theory

2.1 Graphene

2.1.1 Basic properties

Graphene is a two-dimensional structure that consists of one layer of carbon (C) atoms. A carbon atom consists of six electrons, of which two occupy the K shell and the remaining four the L shell. This leads to an electron configuration of $1\mathrm{s}^2 2\mathrm{s}^2 2\mathrm{p}_\mathrm{x} 2\mathrm{p}_\mathrm{y}$. For the formation of hybrid orbitals one of the electrons occupying the $2\mathrm{s}^2$ state is promoted to the $2\mathrm{p}_\mathrm{z}$ orbital. In graphite, the $2\mathrm{s}$, $2\mathrm{p}_\mathrm{x}$ and $2\mathrm{p}_\mathrm{y}$ orbitals are mixed to form three sp^2 hybrid orbitals. The fourth orbital $2\mathrm{p}_\mathrm{z}$ doesn't play any part in this and remains unchanged. Every two overlapping neighbouring sp^2 hybrid orbitals form a very strong σ covalent bond $(\mathrm{C}-\mathrm{C}\,\text{bond})$. These σ bonds all lie in the same two-dimensional plane and connect every carbon atom to three adjacent ones, since every carbon atom has got three sp^2 hybrid orbitals. The remaining $2\mathrm{p}_\mathrm{z}$ orbitals form π bonds with eachother and connect the different two-dimensional carbon layers to form the inter-layer bonds. These π bonds are a lot weaker than the σ bonds. This makes it relatively easy to detach layers of carbon from the graphite. The carbon atoms are arranged in a hexagonal, or honeycomb, structure, which can be seen in the left part of figure 2.1.

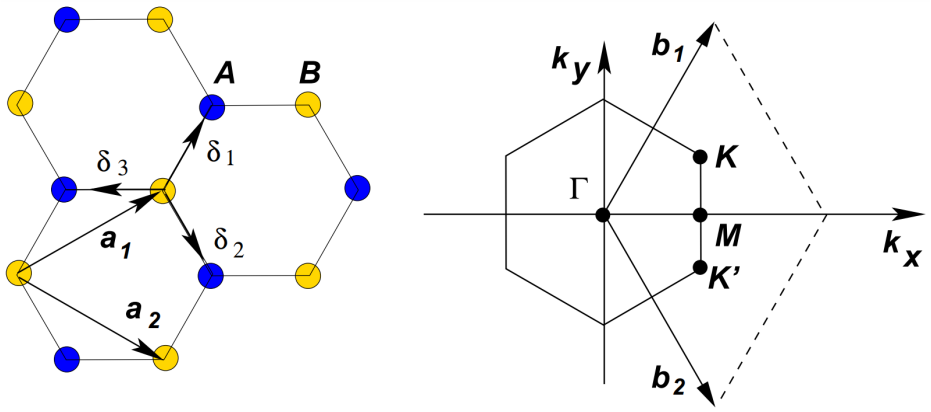

Figure 2.1: In the left side of the figure the honeycomb lattice structure of graphene is pictured. The lattice is made out of two overlapping Bravais sublattices, which are spanned by either the blue or yellow atoms. The primitive lattice vectors are indicated by $\mathbf{a_1}$ and $\mathbf{a_2}$ and the nearest neighbour vectors are labeled by $\boldsymbol{\delta_1}$, $\boldsymbol{\delta_2}$ and $\boldsymbol{\delta_3}$. In the right side of the figure the Brillouin zone of the graphene lattice is shown. The vectors $\mathbf{b_1}$ and $\mathbf{b_2}$ are the primitive vectors of the reciprocal lattice and K and K' are the Dirac points [5].

This lattice is not a Bravais lattice, as its structure cannot be defined by the translation that spans every Bravais lattice

$$\mathbf{R} = n_1\mathbf{a_1} + n_2\mathbf{a_2}, \tag{2.1}$$

where n_1 and n_2 are integers and $\mathbf{a_1}$ and $\mathbf{a_2}$ the primitive translation vectors that should span the entire lattice. However, the graphene lattice can be described by two different triangular Bravais sublattices that overlap with each other. The sublattices are spanned by either the yellow or blue atoms in figure 2.1 with appropriate lattice vectors, labeled with $\mathbf{a}_1$ and $\mathbf{a}_2$. These primitive lattice vectors are given by

$$\mathbf{a}_1 = \sqrt{3}a\left(\frac{\sqrt{3}}{2}\hat{x} + \frac{1}{2}\hat{y}\right) \text{ and } \mathbf{a_2} = \sqrt{3}a\left(\frac{\sqrt{3}}{2}\hat{x} - \frac{1}{2}\hat{y}\right), \tag{2.2}$$

in which a is the distance between two neighbouring carbon atoms, which is about $a \approx 0.142$ nm. Furthermore, one can obtain the vectors that connect neighbouring carbon atoms. These vectors are indicated by $\boldsymbol{\delta_1}$, $\boldsymbol{\delta_2}$ and $\boldsymbol{\delta_3}$ in figure 2.1 and are given by

$$\boldsymbol{\delta_1} = \frac{a}{2}\left(\hat{x} + \sqrt{3}\hat{y}\right) \text{ and } \boldsymbol{\delta_2} = \frac{a}{2}\left(\hat{x} - \sqrt{3}\hat{y}\right) \text{ and } \boldsymbol{\delta_3} = -a\hat{x}. \tag{2.3}$$

The Brillouin Zone of the graphene lattice is shown in the right side of figure 2.1.

The reciprocal lattice vectors are labeled by $\mathbf{b_1}$ and $\mathbf{b_2}$ and are given by

$$\mathbf{b_1} = \frac{2\pi}{3}\left(\hat{x} + \frac{\sqrt{3}}{2}\hat{y}\right) \text{ and } \mathbf{b_2} = \frac{2\pi}{3}\left(\hat{x} - \frac{\sqrt{3}}{2}\hat{y}\right). \tag{2.4}$$

The electronic band structure can be generated by using the tight-binding model. If the self-interaction is set to zero, the first order approximation of this approach gives the following result for the dispersion relation

$$E(\mathbf{k}) = \pm\gamma_0\sqrt{3 + 2\cos\left(\sqrt{3}k_y a\right) + 4\cos\left(\frac{\sqrt{3}}{2}k_y a\right)\cos\left(\frac{3}{2}k_x a\right)}, \tag{2.5}$$

in which γ_0 is the nearest-neighbour hopping energy of graphene. Its value is the same as that found for graphite, which is $\gamma_0 = 3.16\ \mathrm{eV}$. The plus sign represents the conduction band, which has a higher energy, and the minus sign represents the valence band, which has a lower energy. This approximation only describes the π and π^* bands, by far the two most important bands in graphene. The π band describes the valence band, while the π^* describes the conduction band. The points at which equation 2.5 is equal to zero ($E(\mathbf{k}) = 0$) are called the Dirac points or charge neutrality points (CNPs). You can divide them into two separate groups, which correspond to the two sublattices in the graphene structure. These two different groups both have their own notation for every point, namely K and K' in the right side of figure 2.1. For pristine graphene, the Fermi level, also called the chemical potential, is exactly located at the zero-energy level of these Dirac points. In this case the valence band is completely filled, while the conduction band is completely empty.

The full band structure of graphene is shown in figure 2.2, in which not only the π and π^* bands are visible, but also the σ and σ^* bands. The π and π^* bands are closer to the Fermi Level than the σ and σ^* bands. This is a result of the fact that the σ bonds are much stronger than the π bonds, which means that they participate less in bonding. The π bands form so-called canonical valleys in the immediate vicinity of the K and K' points. The eigenenergy equation 2.5 can be rewritten by shifting the origin of the $\mathbf{k}$ space to either the K or K' point, as most of the transitions happen around these Dirac points. Furthermore $\mathbf{k}$ is assumed to be small, as only the vicinity of the Dirac points is of interest.

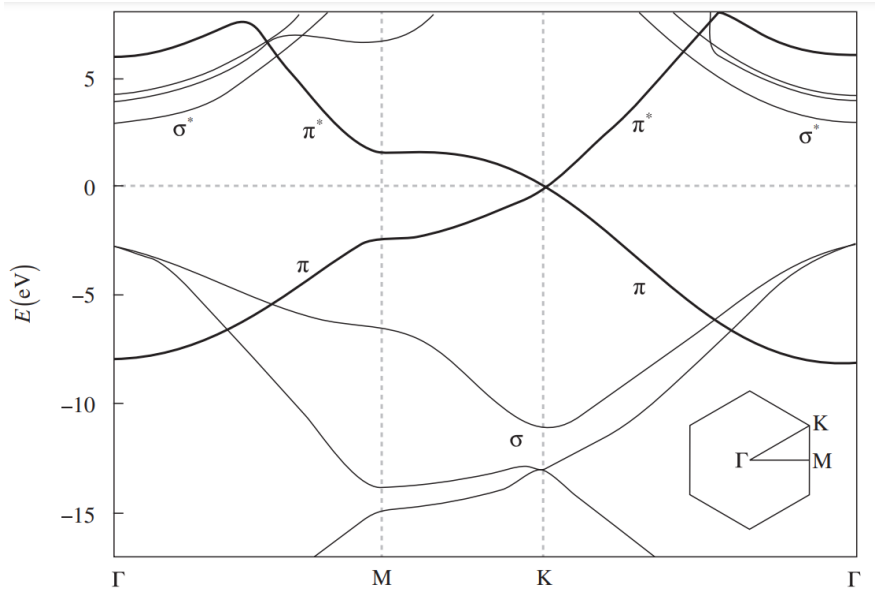

Figure 2.2: Full two-dimensional band structure of graphene, with the thick curves indicating the π and π^* bands and the thin curves the σ and σ^* bands [17].

The eigenenergy equation 2.5 can then be rewritten in the following form

$$E = \pm\gamma_0\sqrt{\frac{9}{4}k_y^2a^2 + \frac{9}{4}k_x^2a^2} = \pm\frac{3}{2}a\gamma_0|\mathbf{k}| = \pm\hbar v_F k, \tag{2.6}$$

in which $\hbar$ is the reduced Planck constant and

$$v_F = \frac{3a\gamma_0}{2\hbar} \approx 1.0 \cdot 10^6 \text{ ms}^{-1} \tag{2.7}$$

is the Fermi velocity in graphene. The result of equation 2.6 means that there is a region around the Dirac points K and K′ in which the dispersion relation of graphene is linear. This phenomenon also appears in the ultrarelativistic limit of a particle. The relativistic dispersion relation of a particle can be written as

$$E = \sqrt{m^2c^4 + p^2c^2}, \tag{2.8}$$

where E is the total energy of the particle, m the mass of the particle, c the speed of light and p the momentum of the particle. In the ultrarelativistic case the energy of the particle is almost completely due to its momentum p. Therefore the m^2c^4-term in equation 2.8 can be neglected, which results in the following equation for the total energy in the relativistic limit:

$$E = pc. \tag{2.9}$$

This is a linear dispersion relation, just like the dispersion relation of graphene in equation 2.6. One could therefore state that the Dirac fermions in graphene act like relativistic particles and can be described by massless fermions with a constant electron velocity. The only major difference is that the Dirac fermions in graphene move with a Fermi velocity v_F that is 300 times smaller than the speed of light c ($\approx 3 \cdot 10^8$ ms^{-1}) [8], [21].

2.1.2 Characterization of graphene

Graphene is a very sensitive material to any external or internal perturbations. This sensitivity could cause problems when setting up an experiment using graphene; while transferring and storing the material the amount of impurities and defects could reach alarming proportions. Its important to chart a graphene layer when using it in an experiment to obtain important information about its quality. The properties of graphene are almost always reported on a substrate [19], such as a silicon/silicon oxide wafer. One way of charting a graphene layer is by carrying out field effect characterization. For this one needs a graphene device with a voltage bias applied to the gate, logically called the gate voltage V_g. This generates an electric field that penetrates the graphene and attracts more carriers from the substrate to the layer of graphene. From the particular voltage at which the carrier is minimum the lowest current is observed. The point with this lowest amount of current is called the Dirac point. For a pristine layer of graphene, so without any defects or impurities, this Dirac point is observed at a gate voltage V_g of exactly 0 V. Another parameter that is often used in field effect characterization is the resistance. The resistance of the graphene is at its maximum at the Dirac point. This is in contrast with a current measurement, which is at its lowest at the Dirac point as already said. If the Dirac point is not exactly found at a gate voltage V_g of 0 V, it means the graphene is not a pristine layer and that it has different properties. It could for instance be doped or heated. Doping the graphene shifts the Dirac point to positive or negative voltages depending on the type of doping. If the Dirac point is shifted to a more positive position, it shows that the doping of the graphene is p-type and vice versa. So if the Dirac point shifts to a more negative position the doping is of the n-type. Several circumstances can cause (unwanted) p-doping of the material. For example, the formation of weak $\mathrm{C-O}$ bonds between a carbon atom in graphene and an oxygen atom in the silicon oxide layer can lead to a p-type conductivity in

graphene; an electron is transferred from the carbon atom to the oxygen atom in silicon oxide. A hole is left behind in the graphene, which leads to an increase in hole concentration in the graphene layer and an forward shift of the charge neutrality point. Moreover, during the fabrication process of a graphene field effect transistor (GFET), whose properties are discussed in more detail in section 3.1, molecules could be adsorbed on the surface channel or at the interface of the graphene and silicon oxide layer. This leads to a forward shift of the Dirac point and a reduction in quality of the graphene device. Therefore polymethyl methacrylate, also known as PMMA, is often used as GFET coverage to prevent further adsorption of certain molecules and the resulting forward shift of the charge neutrality point.
There is also a way to undo this forward shift by annealing the graphene. This is a process of heating up a material until it reaches a temperature at which the physical or chemical properties of the material change. This temperature is maintained for a suitable amount of time inside an oven, after which it is cooled down again to room temperature. It causes the graphene to return its original pristine situation. Annealing the graphene leads to a more or less homogeneous carrier concentration across the sample, which results in a reduction of the width of the peak around the Dirac point [3].
Another feature that is often observed when carrying out field effect characterization is hysteresis. It means in simple words that there is a lag in input and output in a system when the direction is changed. Hysteresis in graphene is the result of charge carries that are trapped and de-trapped between the graphene layer and the silicon oxide layer. The amount of freely moving electrons is therefore reduced which results in a decrease of the electron concentration in graphene. The charge neutrality point is then moved to a more positive gate voltage [25], [23], [22].

2.2 Avalanche photodiode

During the experiment a scintillator will be used that absorbs the energy of incoming electrons and re-emits that energy by the form of light. A multi-pixel photon counter (MPPC) will then be lined up to detect the photons coming from the scintillator. The basic element, named a pixel, of the MPPC consists of several avalanche photodiodes (APDs) and quenching resistors connected in parallel. A schematic structure of the corresponding circuit is shown in figure 2.3.

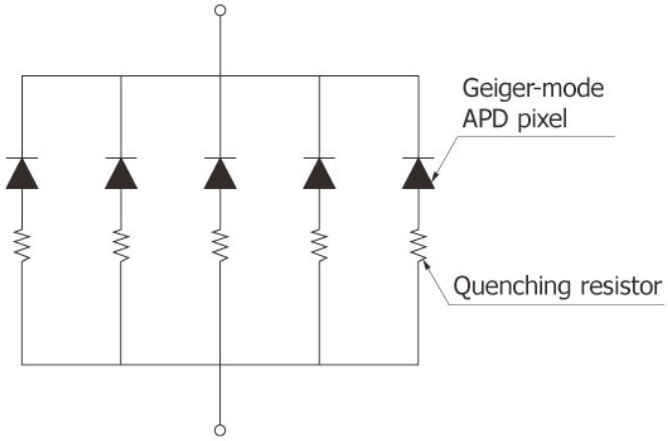

Figure 2.3: Schematic structure of the circuit of an MPPC pixel [9].

A huge number of these pixels are electrically connected and arranged in two dimensions. A closer look on the operation principles of the APD, the main part of a MPPC pixel, will be given below.

2.2.1 PN junction

An avalanche photodiode is a semiconductor photodiode detector that, in this case, uses silicon as the semiconductor in the device to convert light into electricity via the photoelectric effect. Intrinsic crystalline silicon is its most pure state without any doping. It has a steady equilibrium in which neither the positive nor the negative charge carriers have the upper hand. The resistance of intrinsic silicon is too high to operate as a photodiode, so therefore a PN junction needs to be formed in the silicon lattice. It needs to be partially doped with donors to obtain this junction. Donors are atoms of group V of the Periodic Table, which have 5 valence electrons in their outermost shell. This part of the semiconductor then becomes n-type and is called an N region, in which the electrons are the majority charge carriers. The donor atoms form bonds with the silicon atoms and will settle in the lattice structure. However, one of the electrons of the donor atom will remain because of the fact that silicon has only 4 valence electrons compared to the 5 valence electrons of the donor atom. This electron will be donated to the conduction band.
An adjacent part of the material then needs to be doped with acceptors. These are atoms with three electrons in their outermost shell, which are coming from group III of the Periodic Table. As a result, positively-charged holes become the majority carriers in this part of the silicon crystal. The outermost shell of the acceptor atom contains one valence electron less than silicon. The acceptor atom will still settle in

the lattice structure, but has to introduce a hole in the valence band to do so. The dopant atoms now mainly provide the charge carriers in their part of the lattice. This is what is called an extrinsic semiconductor. They typically have a much lower resistance than the intrinsic ones as an increase in majority carrier concentration causes a decrease of the resistance of the silicon. This is because the electrons and holes share the same conduction and valence bands and can move freely through the crystal. This process can be strengthened by applying an electric field across which the charge carriers will drift.
In the resulting PN junction will start to flow a diffusion current; electrons flow from the N region towards the P region and recombine with holes and vice versa. As a result a region between the two sides called the depletion layer, which is depleted from majority carriers, occurs. The majority carriers that drift away leave a donor or acceptor ion behind, which results in a positively-charged depletion layer near the N region and a negatively-charged depletion layer near the P region. This charge difference forms an electric field across the depletion layer pointing towards the negatively-charged part of the depletion layer near the P-region. It therefore opposes the diffusion current which eventually results in an equilibrium. In this equilibrium the electric field cancels the diffusion current, which results in no net carrier flow. A PN junction in its equilibrium is schematically shown in figure 2.4.

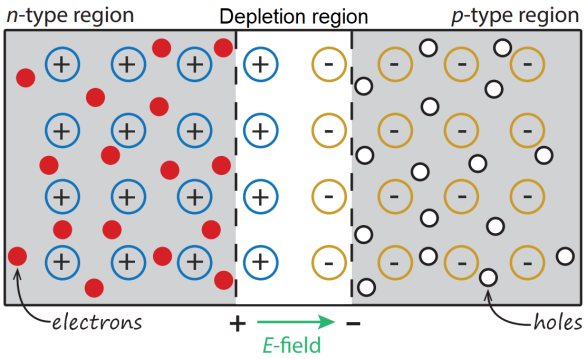

Figure 2.4: PN-junction in equilibrium [18].

The equilibrium in a PN junction can be disturbed by for instance the photoelectric effect; an incident photon carrying an energy that is greater than the bandgap energy of the semiconductor, 1.14 eV in the case of silicon, can promote an electron in the valence band to the conduction band. In figure 2.5 this process is visualized.

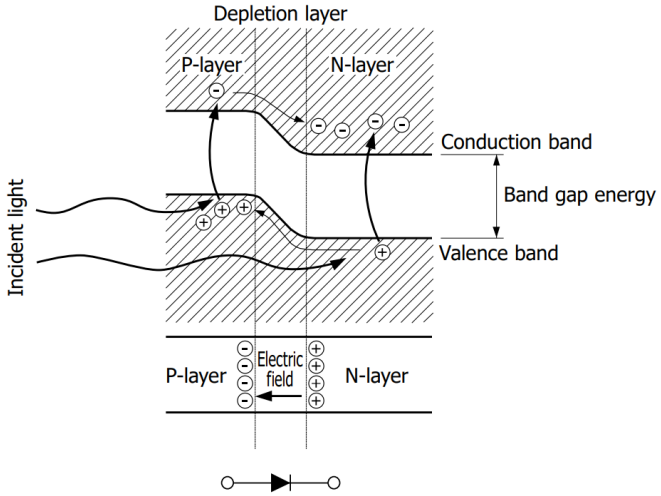

Figure 2.5: Visualization of the silicon band gap [9].

The excited electron and the hole that is left behind in the valence band form an electron-hole pair. If the electron-hole pair is formed inside the depletion layer, the electron will move towards the N side and the hole towards the P side due to the present electric field. If a current loop between the P and N side is formed, the accumulated charge carriers start flowing and induce a current through the loop. If an electron-hole pair is formed outside the depletion layer they will recombine soon after due to the lack of electric field outside the depletion layer.

2.2.2 Reverse bias voltage

One could prevent the recombination of electron-hole pairs formed outside the depletion layer by increasing its depth. If a reverse bias voltage is applied, the electric potential on the N side is set higher than the electric potential on the P side and as a result, the depth of the depletion layer will increase the amount of electron-hole pairs inside this layer. Consequently, the electric field in the depletion layer will become stronger. Charge carriers will therefore gain more kinetic energy before a possible collision with an atom in the lattice. If the kinetic energy becomes bigger than the bandgap energy of silicon, a collision of that carrier with an atom could cause the formation of another electron-hole pair. This could lead to a rapid increase in the amount of carriers, which is named an avalanche. The exact amount of increase is expressed by a quantity called the gain. A relation between the applied reverse bias voltage and the gain of a typical APD is given in figure 2.6.

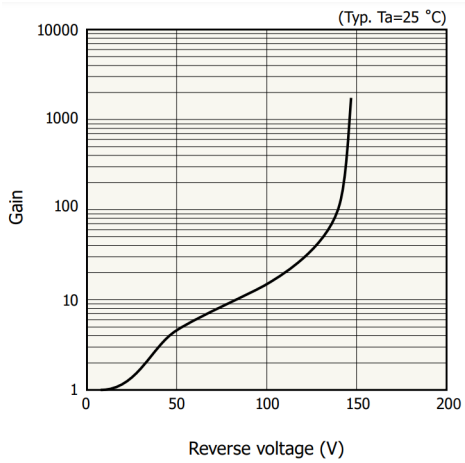

Figure 2.6: Plot of the gain of an APD versus the reverse bias voltage V [9].

Between 50 en 100 V the graph approximately has a linear slope. The gain and applied reverse bias voltage therefore have a $10^{\alpha V}$ relationship. From 100 V onward, the slope suddenly starts increasing a lot. The value of the reverse bias voltage at which this happens is called the breakdown voltage V_{BR} of the APD. If the applied reverse bias voltage is higher than this breakdown voltage, the APD is operating in Geiger-mode. To eventually stop this discharge, a quenching resistor is connected in series with the APD, as again can be seen in figure 2.3. If the discharge flows through this resistor it causes a drop in the operating voltage of the APD [9].

2.3 Field effect transistor

A field effect transistor (FET) is a transistor that controls the current flow in a semiconductor by the use of an electric field. A FET usually has a semiconductor channel and three terminals: the source (S), drain (D) and gate (G). Through the source the charge carriers, electrons or holes, enter the channel. The drain is the terminal through which the charge carriers leave the channel. The current can be controlled by applying a current to the gate. This current alters the conductivity σ between source and drain. This applied potential together with the potential applied across the source terminals affect the size of this so-called conductive channel, through which the electrons flow from source to drain. There are many different types of FETs available. One of them is the graphene field effect transistor (GFET), which is used during the experiments. In section 3.1 a closer look will be taken on this transistor [4].

CHAPTER 3

Materials

During the experiments a few different devices were used that need further explanation to fully understand their working mechanisms. These instruments will be outlined and explained in detail in the sections below.

3.1 Graphene field-effect transistor chip

Graphene field-effect transistors have the typical field-effect transistor look, as explained in section 2.3, with a very small graphene channel inserted between the source and drain. The type of GFET that is used in this experiment is called a GFET-S10, fabricated by Graphenea. The graphene is obtained by chemical vapor deposition (CVD) of a carbon source at very high temperatures. The extracted carbon atoms are laid down on the substrate and will eventually form the characteristic hexagonal graphene lattice structure. This layer of graphene is then transferred from this deposition substrate onto a wafer which in this case is made of silicon (Si). Metal electrodes are located onto this layer of graphene to serve as the interface between the graphene and the stimulating devices like a power supply. The contacts of the GFET-S10 devices are gold-based and are indicated in figure 3.1, which shows the entire cross-section of one GFET-S10 device. The channels in the GFETs have unprecedented sensitivity because of the structure of graphene, being one layer of atoms thick. This is a huge benefit over the standard FETs, because most of the channels in those devices are three-dimensional. This could limit the respond sensitivity of such devices drastically, as a change of the electric charge at the surface doesn't necessarily mean that it will penetrate further into the channel. The two-dimensional graphene channel, on the other hand, is always exposed as a

whole to its surroundings.

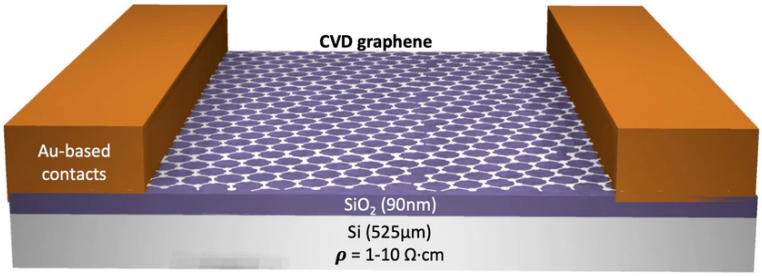

Figure 3.1: GFET-S10 chip device cross-section [11].

One GFET-S10 chip provides 36 devices that are distributed in a grid pattern. 30 of those devices have a Hall-bar geometry while the other six have a 2-probe geometry. A lay-out of the chip is shown in figure 3.2. The 36 devices are arranged in six columns of six devices. The first 5 columns contain the Hall-bar devices and the last column contains the 2-probe devices [4].

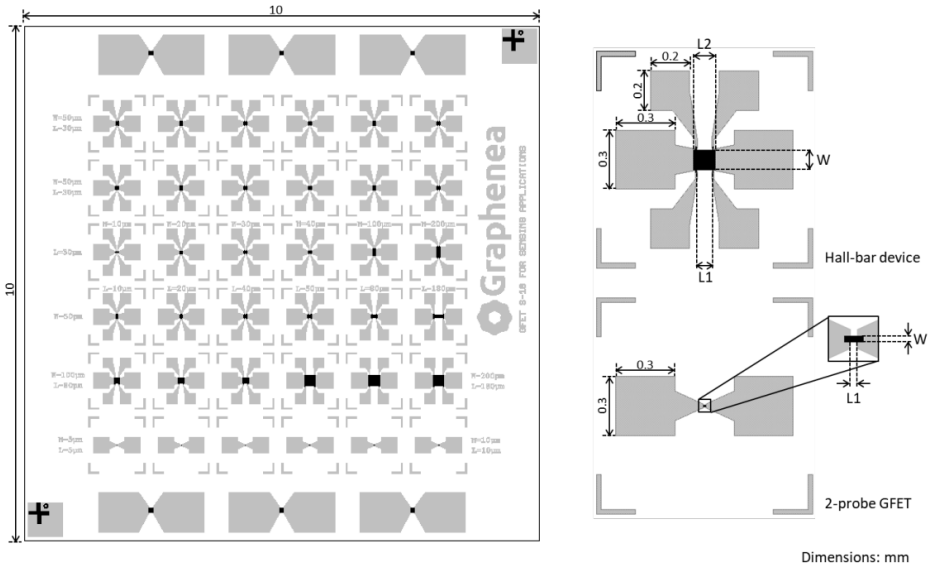

Figure 3.2: GFET-S10 chip with the 36 different devices. The dimensions of the graphene channels vary per device. Right next to the chip a single Hall-bar device and 2-probe device are shown [13].

Graphenea did some measurements on the transfer curve characteristics of the GFET-S10 itself. They measured at a source-drain voltage V_{SD} of 20 mV, at room temperature and under vacuum conditions. They included their results in a plot in the data sheet, which is given in figure 3.3.

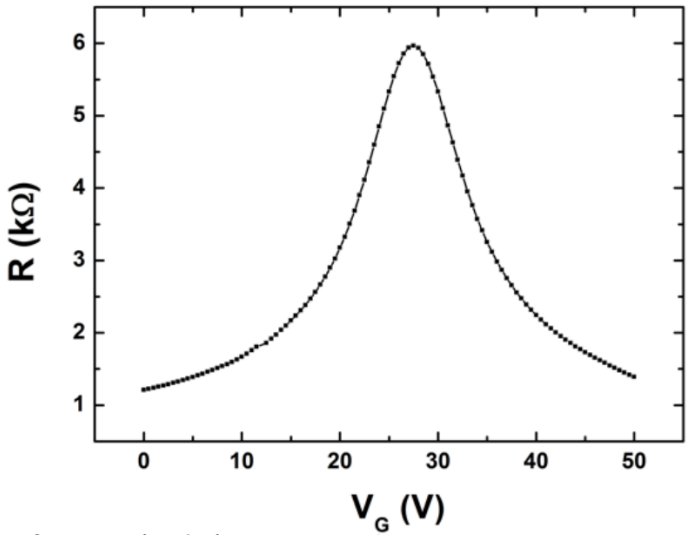

Figure 3.3: Transfer curve from the GFET-S10 datasheet of a device with a width and length of 50 μm, measured at a source-drain voltage V_{SD} of 20 mV, at room temperature and under vacuum conditions [12].

3.2 Scintillator

A scintillator is a certain material that exhibits scintillation. Scintillation is a flash of light produced in a transparent, fluorescent material when it's bombarded by a certain type of radiation. It absorbs the energy of the incoming particle and re-emits that energy by the emission of photons. The number of photons that are emitted by the scintillator is proportional to the amount of energy carried by the incoming particle. In the experiment the EJ-208 scintillator from Eljen Technology is used; a plastic scintillator that can be fully customized to the preferred geometries. The wavelength of maximum emission λ_{max} is 435 nm, as can be seen in the emission spectrum of the EJ-208 scintillator in figure 3.4. It also has a high light attenuation length of 400 cm, which will decrease the probability that an emitted photon is again absorbed by the material.

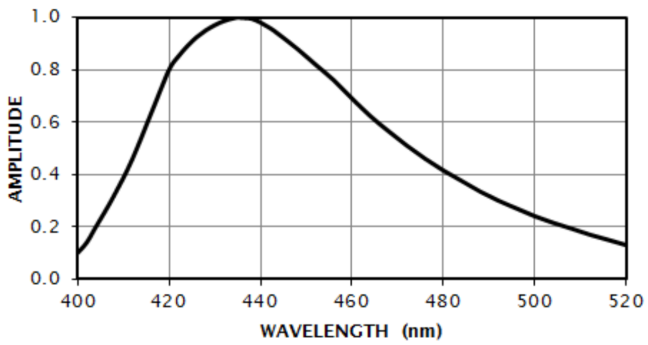

Figure 3.4: Emission spectrum of the EJ-208 scintillator [7].

3.3 Multi-Pixel Photon Counter

A MPPC, short for multi-pixel photon counter, is a device that is called a silicon photomultiplier (SiPM). Their basic operation principles are already described in section 2.2. The avalanche photodiode operates in Geiger-mode with a sufficient reverse bias voltage applied. Each single pixel is then sensitive to a single photon. The MPPC that is used in this experiment is the S13360-1350CS, fabricated by Hamamatsu. The photon detection efficiency (PDE) is a quantity expressed in percentages and gives an indication of the amount of photons that are detected compared to the number of incident photons. This particular SiPM has a maximum PDE at a wavelength of approximately 450 nm, which can be seen in the plot in figure 3.5, that gives the relation between the PDE in $\%$ and the wavelength in nm. This comes close to the wavelength of maximum emission λ_{max} of 435 nm of the EJ-208 scintillator.

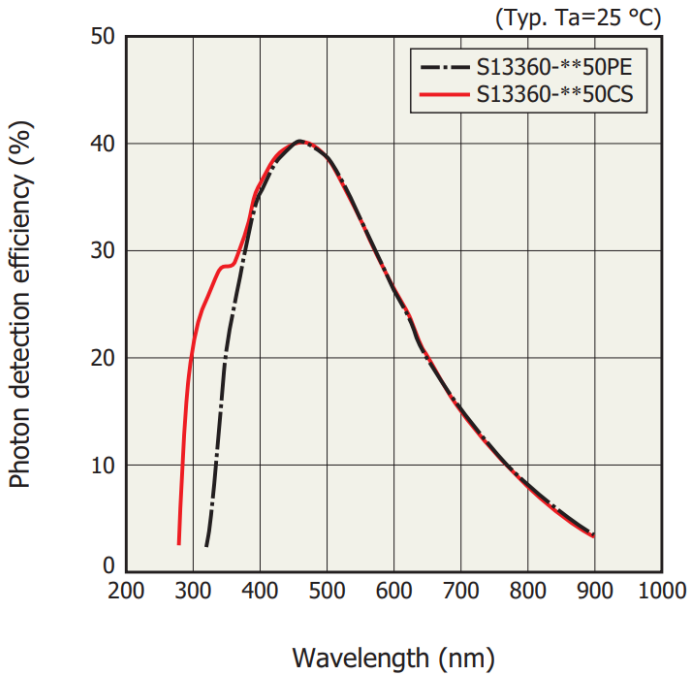

Figure 3.5: Relation between the photon detection efficiency (in $\%$) and the wavelength (in nm) of the silicon photomultiplier. The red line corresponds to the S13360-**50CS series, including the S13360-1350CS [14].

The MPPC suffers from different kinds of noise. For instance, there will be an average rate of registered counts that are not related to any incoming photon signals and occur randomly. These pulses cause detection errors and are called dark pulses. The number of these pulses that is observed by the MPPC is referred to as the dark count. A second type of noise is coming from avalanche carriers that get trapped in impurity energy levels. If these carriers absorb the right amount of energy to reenter

the conduction or valence band, they will produce pulses that arrive with a delay compared to the original pulse. That is why they are called afterpulses. A third type of noise that could disturb the output of the MPPC is called crosstalk. A pulse as a result of crosstalk occurs when a pixel that detects a photon affects surrounding pixels. These pixels will then produce a pulse as well without detecting a photon. The crosstalk varies with the operating voltage; increasing the overvoltage results in a higher crosstalk probability. However, it also improves the photon detection efficiency and increases the gain. The operating voltage therefore needs to be chosen carefully. The relations between these characteristics and the operating voltage are shown in figure 3.6.

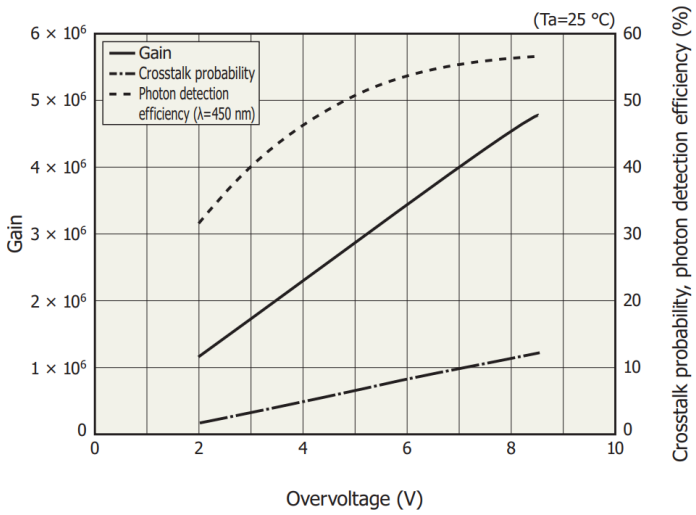

Figure 3.6: Specifications of the gain, crosstalk probability and photon detection efficiency at an certain overvoltage V of devices with a pixel pitch of 50 μm, including the S13360-1350CS, measured at a temperature Ta of 25 °C [14].

3.4 MPPC evaluation circuit

To measure the output current of the MPPC, an evaluation circuit is needed. The evaluation circuit that is used in the experiment is the C12332-01 produced by Hamamatsu and consists of two main parts that are coupled: the sensor circuit board and the power supply circuit board. The MPPC can be mounted in a socket that is present on the sensor circuit board. The operating voltage of the MPPC is provided by a power supply C11204-01 on the power supply circuit board. Therefore an external power supply needs to be connected and supply $\pm$ 5 V. Via an USB cable the power supply circuit board can be connected to a PC, which has to have the right sample software installed. With this software the operating voltage of the MPPC

can be set. There is also an analog signal cable connection on the power supply circuit board that can connect the board to an oscilloscope, which can be used to read out the output current of the MPPC [15].

3.5 Radioactive source

The radioactive source that has been used in the experiment is Strontium-90 (^{90}Sr). For the actual PTOLEMY experiment the isotope Tritium (T) will be used. However, tritium is hard to manufacture and therefore very costly. Strontium is an alkaline earth metal with four naturally occurring isotopes, but Strontium-90 isn't one of them. It is a by-product of nuclear fission. The isotope undergoes β^- decay; it emits an electron e^- and an electron antineutrino ν^- via the following decay reaction:

$$^{90}_{38}Sr \longrightarrow {}^{90}_{39}Y + e^- + \bar{\nu}_e. \tag{3.1}$$

It has a half-life $t_{\frac{1}{2}}$ of 28.79 years, distributing a decay energy of 0.546 MeV in the process to the electron e^-, electron antineutrino $\bar{\nu}_e$ and the isotope yttrium $^{90}_{39}$Y. This isotope is radioactive as well and again undergoes β^- decay, resulting in the following decay reaction:

$$^{90}_{39}Y \longrightarrow {}^{90}_{40}Zr + e^- + \bar{\nu}_e. \tag{3.2}$$

The decay energy of $2.28\ \mathrm{MeV}$ is again distributed to an electron e^- and its antineutrino $\bar{\nu}_e$, and the stable isotope Zirconium $^{90}_{40}$Zr, with the half-life $t_{\frac{1}{2}}$ of this reaction being 64 hours [6].

3.6 Vacuum desiccator

A vacuum desiccator is a sealable enclosure that is used to store moisture-sensitive items in a vacuum. The vacuum inside the desiccator is created by a stopcock that is applied on the enclosure and ensures rapid drying of the product that is being stored inside. Due to the adsorption of water molecules the graphene on the SiO_2 is often p-doped when it is exposed to the open air. As a result the Dirac point shifts towards more positive voltages and could even reach a point outside the recommended gate voltage range. To prevent this from happening, the graphene chips will be stored inside a vacuum desiccator when not in use.

CHAPTER 4

Methods

A few different steps need to be taken to be able to reach the end goal of detecting a beta particle with the aid of graphene. First one needs to make sure the graphene chip is working properly. That means a stable transfer curve needs to be measured. If this first step has been taken, the next step is to detect a beta particle with the aid of a silicon photomultiplier. If this has been done, one can implement the graphene chip into the silicon photomultiplier setup and see if there is an agreement between the transfer curve measurements and the silicon photomultiplier data.

4.1 Measuring the transfer curve

The first important step that needs to be taken is to measure a stable transfer curve of a graphene chip. An incoming beta particle should cause a small perturbation of the transfer curve. Without a stable resistance output it will be very hard to observe such a small perturbation. In the subsections below there are two methods described to obtain a stable transfer curve.

4.1.1 Probe setup

The first set up that was used to try and measure the transfer curve of a piece of graphene is called the *Probe setup*. To connect the contacts of a GFET-S10 device with the appropriate equipment, a probe with four metal pins is designed to make contact with the four contact points of the Hall-bar devices. The appropriate voltage or current can be applied with the use of the wires that are connected to the metal pins, as can be seen in figure 4.1.

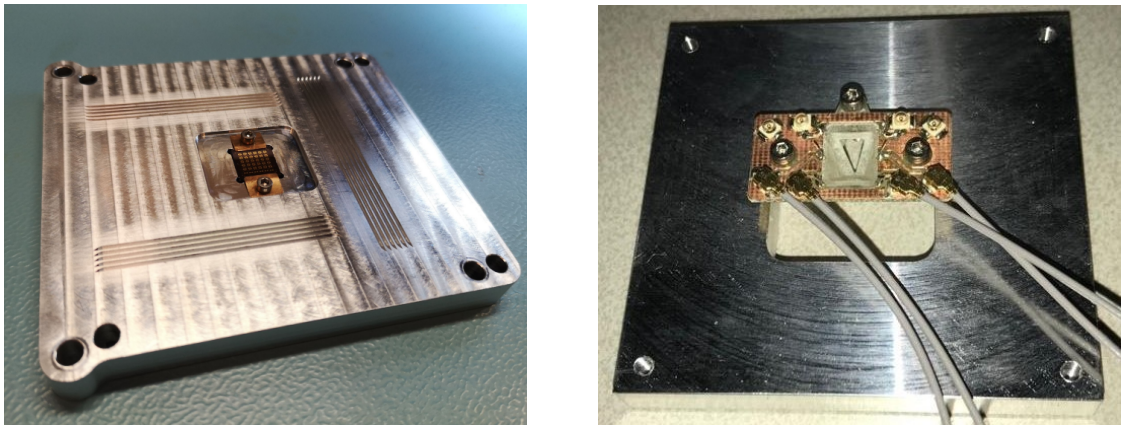

(a) (b)

Figure 4.1: (a) The metal plate that serves as the placeholder of the graphene chip. The graphene chip is the small blue chip in the middle which is kept in its place by two small copper plates. The horizontal and vertical grooves are also visible. (b) Metal plate with the probe attached to it. The gray wires lead to the appropriate equipment.

The probe is fastened on a metal plate, that has some relief at the bottom of it. Another metal plate has been designed especially for this setup to serve as a holder for the GFET-S10 chip. In the middle the metal has been carved out in the exact shape of the GFET-S10 chip. The chip itself is then placed in this spot and secured with small copper plates to prevent the slightest bit of movement. Several grooves have been made in the metal, which match perfectly with the relief of the metal plate of the probe. By putting the plate of the probe exactly on these grooves, the pins are perfectly placed above one of the 30 Hall-bar devices. The metal plate with the GFET-S10 chip has exactly five horizontal and six vertical grooves, corresponding to the 5 times 6 different Hall-bar devices. To place the probe correctly above one of the Hall-bar devices a microscope is used. The metal plate with graphene chip is laid underneath to check whether the four pins are placed exactly at the contact points of the Hall-bar device. The sample is then connected via the wires to eventually create the setup that is schematically shown in figure 4.2. Between the two outer contacts, the source and the drain, a so-called source-drain voltage V_{SD} is applied, which is grounded at one side. This voltage enables the transport of charge carriers through the graphene sample. It has an associated current, the source-drain current I_{SD}, which is measured by a multimeter. This multimeter is connected in series to the power supply of the source-drain voltage. Beside that, a gate voltage V_G is applied to the silicon substrate. This gate voltage creates an electric field on the graphene sample and modulates its conductivity. In addition to that, the volt-

age V_{12} is measured directly across the graphene sample by a multimeter using the two inner contacts. A major benefit of this way of measuring is that the resistance of the graphene channel alone is obtained. By measuring the voltage between the two outer contacts, a potential voltage drop at the graphene-metal interface could cause an inaccurate result. Its resistance also doesn't depend on the gate voltage V_G in the same way as the graphene channel resistance itself. Greater sensitivity to an applied gate voltage can therefore be achieved by measuring the voltage directly over the inner contacts.

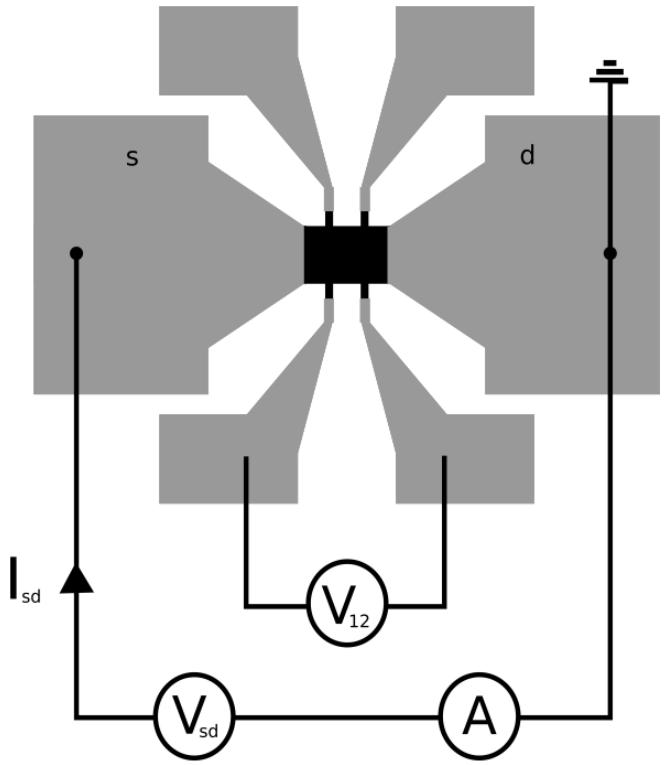

Figure 4.2: Schematic representation of the setup that is used to do measurements on the transfer curve of the GFET-S10 device [12].

A steady source-drain voltage V_{SD} of 20 mV was applied between the source and drain. In addition, a gate voltage V_G, starting from 0 V, was applied and increased up to 50 V. The GFET-S10 chip was then removed from the setup and stored in a case in which it was delivered to prevent unwanted interactions of the graphene with its surroundings. A few days later these measurements were repeated and done on the same device, to see if the graphene sample can produce a steady transfer curve. After repeating the measurements it became clear that a lot of GFET-S10 devices stopped working. In the end a point of no working devices was reached and a new chip needed to be ordered. The exact same chip was ordered, but it appeared to have not the exact same dimensions as the old one. The difference was not even

noticeable with the naked eye, but it didn't fit in the carved out spot in the metal plate. It therefore was cut as careful as possible to the correct dimensions. The exact same measurements were done on this new chip, but that didn't work either. The two chips were therefore checked under a microscope and it turned out that they were unusable.

4.1.2 Chip carrier setup

After checking the graphene chips under a microscope and inspecting the pictures, it was obvious that the *Probe setup* needed to be reconsidered whether it is the most effective way to obtain a stable transfer curve. In the end there was decided to ignore the setup and start working on a new one: the *Chip carrier setup*, which contains a chip carrier as a holder of the graphene. There were again two new GFET-S10 chips, produced by Graphenea, ordered. However, this time they were asked to cleave the chips along the black lines in figure 4.3.

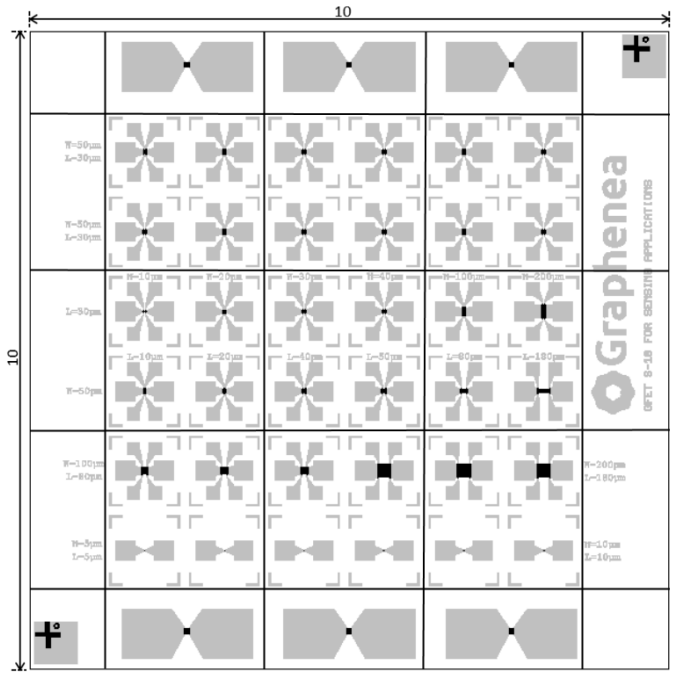

Figure 4.3: GFET-S10 chip with the black lines, dividing the relevant part of the chip in nine pieces, representing the lines along which the chip has been cleaved.

This would make each piece fit perfectly inside the chip carrier. However, they were not able to do that. They were therefore asked to leave a layer of PMMA on top of the chips before shipping them. This will lower the risk of damage when cutting the chips without their help. After the chips were successfully cleaved, the small GFET-S10 parts were all stored in a vacuum desiccator that was ordered. They only

leave the desiccator when they are needed during the experiments. After a part of the GFET-S10 chip was placed in the chip carrier and connected properly, the transfer curve measurements could start again. Firstly, a chip with a PMMA layer on top was placed in the chip carrier. The gate voltage V_g was then swept back and forth, starting and ending at $0\ \mathrm{V}$. After removing the PMMA layer these measurements were done under the exact same conditions. Then the graphene chip was annealed inside an oven. Firstly the annealing temperature was set on $400\ \mathrm{K}$. After the transfer curve measurements were taken, the graphene was again annealed at an annealing temperature of $450\ \mathrm{K}$. This is also the maximum temperature rating of the GFET-S10. Higher temperatures would improve the quality of the graphene even more, but it would also be harmful for the chip.

4.2 Detecting beta particles with the silicon photomultiplier

To check if a change in the resistance of the GFET-S10 device is the result of an incident beta particle, a silicon photomultiplier is used; if the pulse produced by the SiPM agrees with the change in the resistance of the graphene, one could say that a beta particle is detected with the help of a GFET-S10 device. To make that happen one needs to make sure the SiPM works properly by trying to detect a beta particle without any graphene implemented into the setup yet. The MPPC is therefore mounted in a socket on the sensor circuit board of the C12332-01. A power supply is connected to the power supply circuit board and supplies $\pm\ 5\ \mathrm{V}$. This board is also connected to a PC with the appropriate software installed to set the operating voltage. The optimal reverse bias voltage for this specific MPPC is V_{BR} + 3 V, according to its datasheet. To determine the breakdown voltage V_{BR} one needs to look for the reverse bias voltage that leads to Geiger discharge. When the breakdown voltage has been found, the scintillator and the source are aligned with the SiPM. The source emits beta particles which penetrate the scintillator. As a result, the scintillator emits photons that are detected by the SiPM. It produces a pulse which is displayed on an oscilloscope connected to the power supply circuit board if the trigger level is set. The setup as a whole is shown in figure 4.4.

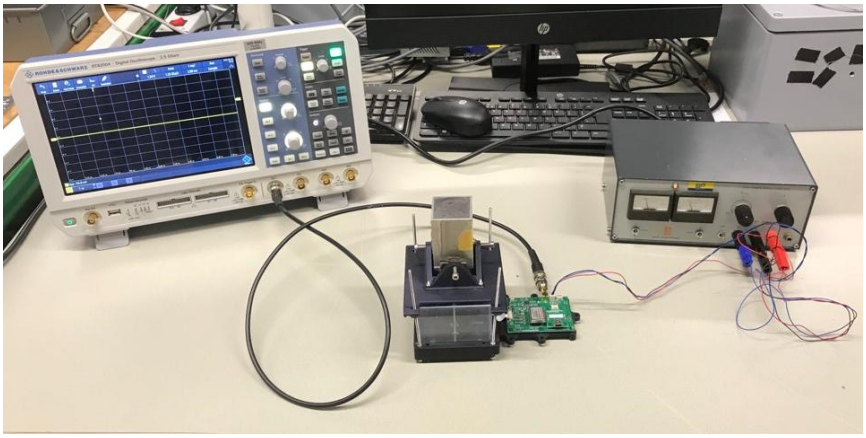

Figure 4.4: Silicon photomultiplier setup with the oscilloscope to the left, connected to the green power supply circuit board in the middle. This circuit board is connected to the sensor circuit board, which is located underneath the scintillator next to the power supply circuit board. The gray Strontium-90 source is placed on top of the scintillator. The external power supply to the right applies the $\pm$ 5 V.

These measurements were done in a lab which was made as dark as possible to prevent any unwanted incident photons reaching the SiPM. There is also a special metal box designed, which is shown in figure 4.5, to operate as an even better protector from unwanted incident photons. The right connections were made to the sides of the box so that the setup can also operate inside the box. After the setup was placed inside the box, the edges were covered with tape to make sure no other light could penetrate the box.

Figure 4.5: Metal box that protects the setup from unwanted incident photons.

4.3 Using graphene as a beta particle detector

Unfortunately, due to the lack of detection of beta particles by the silicon multiplier the graphene chip hasn't been implemented into the setup yet.

CHAPTER 5

Results

5.1 Measuring the transfer curve

As already stated above, the transfer curve of the graphene has been measured using two different setups. The results obtained from both of these setups are stated in the the following subsections.

5.1.1 Probe setup

With an applied source-drain voltage V_{SD} of 20 mV, the resistance of the GFET-S10 was determined by measuring the source-drain current I_{SD} over the outer contacts and the voltage V_{12} over the inner contacts at room temperature. The results as a function of the gate voltage V_g are shown in figure 5.1.

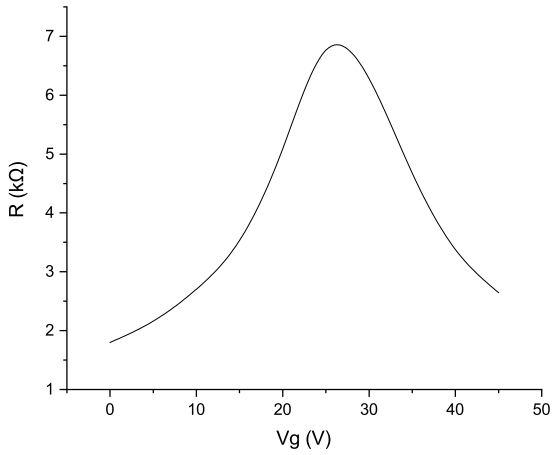

Figure 5.1: Transfer curve measurements of a GFET-S10 device, measured at room temperature and at a source-drain voltage V_{SD} of 20 mV.

After it became clear that a lot of the GFET-S10 devices weren't working properly, the two chips were put underneath a microscope to have a closer look at the single GFET-S10 devices. One of the pictures that was taken by the microscope can be seen in figure 5.2. All kind of scratches are visible both on the contact points and the layer of graphene itself.

Figure 5.2: A microscopic picture of a GFET-S10 device after it was used to do measurements in the *Probe setup*.

5.1.2 Chip carrier setup

The first measurements were done at room temperature with the PMMA layer still on top of the GFET-S10 device. The gate voltage was swept between -60 V and 70 V, starting and ending at 0 V. The resulting measurements of the resistance R are

plotted as a function of the gate voltage V_g, as can be seen in figure 5.3.

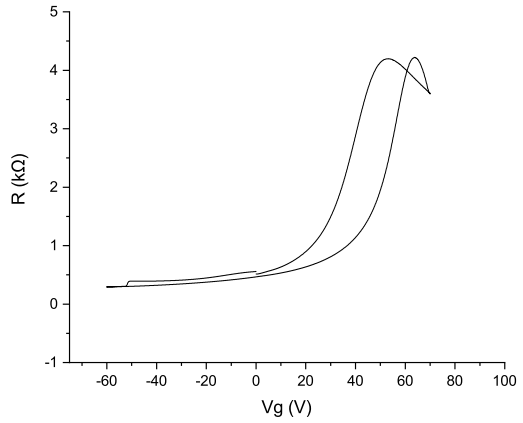

Figure 5.3: Transfer curve measurements of a GFET-S10 device with a layer of PMMA on top. The gate voltage V_g was swept between -60 V and 70 V, starting and ending at 0 V. These measurements were done at room temperature.

The Dirac point in the forward sweep is located at a gate voltage V_g of approximately 53,2 V, while the Dirac point in the backward sweep is located at a gate voltage V_g of approximately 63,6 V.
After removing the layer of PMMA these measurements were done under the exact same conditions. The gate voltage was swept between -20 V and 70 V, starting and ending at 0 V. The resulting measurements of the resistance R are plotted as a function of the gate voltage V_g, as can be seen in figure 5.4.

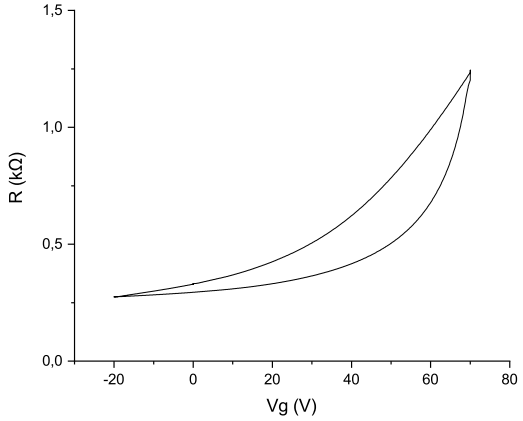

Figure 5.4: Transfer curve measurements of a GFET-S10 device without a layer of PMMA on top. The gate voltage V_g was swept between -20 V and 70 V, starting and ending at 0 V. These measurements were done at room temperature.

The Dirac point is located at a gate voltage V_g higher than 70 V, approximately around 80 V. Unfortunately, a higher gate voltage could not be applied.
After annealing the GFET-S10 chip at a temperature of 400 K, the measurements were repeated. The gate voltage was swept between -30 V and 60 V, starting and ending at 0 V. The resulting resistance R values are plotted as a function of the gate voltage V_g in figure 5.5.

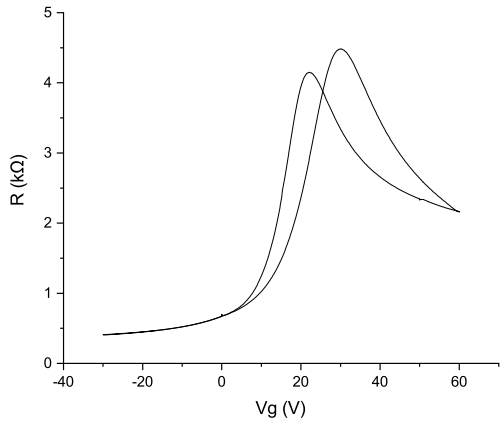

Figure 5.5: Transfer curve measurements of a GFET-S10 device without a layer of PMMA on top after annealing the chip at a temperature of 400 K. The gate voltage V_g was swept between -30 V and 60 V, starting and ending at 0 V.

The Dirac point in the forward sweep is located at a gate voltage V_g of approximately 22,2 V, while the Dirac point in the backward sweep is located at a gate voltage V_g of approximately 30,0 V.
Thereafter, the GFET-S10 chip was annealed at a temperature of 450 K. The gate voltage V_g was swept several times between -30 V and 50 V, starting and ending at 0 V. Only the resulting transfer curve of the first sweep is shown in figure 5.6 on the next page.

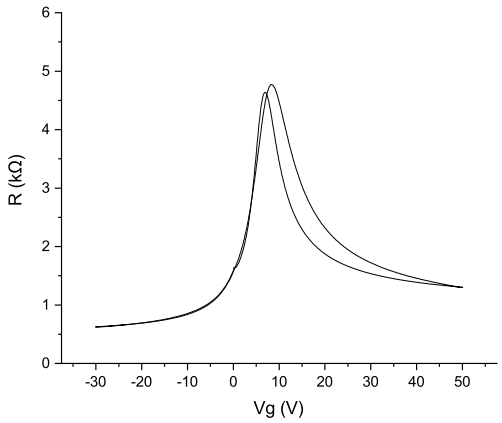

Figure 5.6: Transfer curve measurements of a GFET-S10 device without a layer of PMMA on top after annealing the chip at a temperature of 450 K. The gate voltage V_g was swept several times between -30 V and 50 V, starting and ending at 0 V. Only the first sweep is shown in this plot.

The Dirac point in the forward sweep is located at a gate voltage V_g of approximately 6,9 V, while the Dirac point in the backward sweep is located at a gate voltage V_g of approximately 8,3 V.

5.2 Detecting beta particles with the silicon photomultiplier

Despite the fact that the data sheet already gives a value for the breakout voltage V_{BR}, it is always sensible to check this by yourself. The breakout voltage V_{BR} is therefore determined by slowly increasing the reverse bias voltage. The resulting breakout voltage is 52,9 V. Not a single attempt to detect a beta particle with the silicon photomultiplier has been successful yet.

5.3 Using graphene as a beta particle detector

The graphene chip hasn't been integrated into the setup yet, as a consequence of the lack of detection beta particles with the scintillator setup.

CHAPTER 6

Conclusion and Discussion

At first sight, the probe setup gave some very promising results of the transfer curve of the graphene chip. The results, which are shown in figure 5.1, matched the transfer curve measured by Graphenea, given in figure 3.3, quite well. It looked like the graphene chip operated well at room temperature. It resulted in a glance of hope; maybe the transfer curve of the graphene chip at room temperature is that stable that it isn't necessary to measure at vacuum conditions or to flush it with helium or argon.
However, the follow-up measurements weren't quite as promising. After the power supply was replaced with a power supply that could go up to 60 V, the exact same measurements gave some fluctuating results. It looked like the resistance of the graphene chip was increased in the meantime. Being in contact with the air eventually did result in doping of the graphene. It showed that these measurements aren't replicable under these circumstances. More follow-up measurements confirmed this statement; a reasonable transfer curve eventually wasn't obtained anymore. This resulted in the idea to replicate the measurements inside a box flushed with argon or helium.
However, before this idea was worked out the graphene chip stopped working. Every single device appeared to be broken. That fear was confirmed when a microscope was used to have a closer look at the single devices on the GFET-S10 chip; scratches were visible all over the contacts and even went through the graphene. One of the pictures that was taken by the microscope is shown in figure 5.2. During the measurements the 2-probe devices haven't been used at all. This has resulted in a clear difference between the state of the contacts of the 2-probe devices and the Hall-bar devices, which indicates that the damage that has been taken is mainly

coming from the *Probe setup*. The state of the second chip, that was ordered after the first original chip stopped working, was even worse; additional scratches were visible on the entire surface. In hindsight, the process of cutting the second chip to the correct form should have been done more carefully.
Because these observations clearly indicated that the current *Probe setup* was useless for measuring a stable transfer curve, a few alternatives could be considered. The exact placement of the pins could for example be reconsidered. Another option is to provide the pins with strings, which compensate the pressure when there is too much applied. This could prevent the contact points from being damaged by the pressure of the pins. In the end, there were too many uncertainties regarding these alternatives. Therefore, there has been decided to ignore the *Probe setup* from this point onward and to choose for a much safer *Chip carrier setup*.
When looking at the results obtained at room temperature of the GFET-S10 devices shown in figure 5.3 and 5.4, one main difference stands out: the Dirac point of the device without the PMMA layer on top is shifted much further to the right. PMMA prevents the adsorption of certain molecules on the surface of the channel or at the interface between the graphene and silicon oxide layer. An electron is then transferred from the graphene to the adsorbed molecule, which leaves a hole behind in the graphene. As a result, the graphene becomes p-doped and the charge neutrality point is shifted toward a more positive gate voltage.
A second important feature that is observed in both of these plots is a clear and visible hysteresis. This is due to the fact that charge carriers are trapped and detrapped at the interface of the graphene layer and the silicon oxide layer. Because of this freely moving electrons appear less in the graphene layer, which results in a decrease of the effective electron concentration. The graphene layer is therefore more p-doped than before, which causes the charge neutrality point to move to a more positive gate voltage when reducing the gate voltage back to zero.
After annealing the chip at a temperature of 400 K, the charge neutrality point shifted toward the zero gate voltage as can be seen in figure 5.5; a huge difference when comparing it to the location of the charge neutrality point of the same device measured at room temperature that is shown in figure 5.4. The annealing process removes impurities of the graphene surface such as moisture. These impurities act as p-dopants, which results in a positive shift of the charge neutrality point. So by removing these impurities due to the annealing process, a negative shift of the charge neutrality point is visible.
After 450 K annealing, the charge neutrality point is even further shifted toward the zero gate voltage, as can be seen in figure 5.6. This is because at these temperatures

even more moisture is evaporated, leading to a decrease in the amount of impurities in the device. A second important observation is that the transfer curve exhibits weaker hysteretic behaviour. The adsorbates such as water act like charge traps, which results in the hysteretic behaviour. Removing these impurities by annealing the graphene device results in this weaker hysteretic behaviour.
Looking at all the transfer curves at once shows that the charge neutrality point is located at a positive gate voltage in every single case. It means that the graphene is unintentionally p-doped. For the device not covered with PMMA at room temperature, the charge neutrality point was even located behind the sweeping upper limit of 70 V. Annealing the graphene chip undoes the p-doping of the material, which results in a negative shift of the charge neutrality point. There is also a difference in width of the charge neutrality point peaks observed before and after annealing; the transfer curve after 450 K annealing, given in figure 5.6, has a reduced width of its charge neutrality point peak compared to the other results. It is a result of the better homogeneity after annealing the sample; the carrier concentration is more or less the same across the sample, which results in less fluctuations of the transfer curve. Annealing the chip improves the quality of the graphene device and is therefore recommended when trying to obtain a steady transfer curve.
Unfortunately, the attempts to detect a beta particle in the silicon photomultiplier setup haven't given any optimistic results yet. The problem probably originates from the scintillator that is used; it looks like it emits photons with a wavelength that differs too much from the maximum photon detection efficiency of the MPPC. The best way to solve this problem is to look for a scintillator which produces light with a wavelength value as close to the maximum photon detection efficiency as possible. In the end it shouldn't take too many effort to detect a beta particle with the silicon photomultiplier setup. When this is accomplished, the graphene chip can be implemented in the setup. The promising measurements of the transfer curve indicate that it should be possible to detect small fluctuations coming from an incident beta particle.
In terms of how far along the way the world is when it comes to understanding the true properties of this magical material, this is just the tip of a huge iceberg. It needs to spend a lot more time doing research to truly understand what makes graphene such a magical material, before it will be integrated in the applications in which one believes it will eventually flourish.

Bibliography

[1] E. Baracchini et al. Ptolemy: A proposal for thermal relic detection of massive neutrinos and directional detection of mev dark matter, 2018.

[2] M.G. Betti et al. Neutrino physics with the PTOLEMY project: active neutrino properties and the light sterile case. *Journal of Cosmology and Astroparticle Physics*, 2019(07):047–047, jul 2019.

[3] K.I. Bolotin et al. Ultrahigh electron mobility in suspended graphene. *Solid State Communications*, 146(9-10):351–355, 2008.

[4] Miklos Bolza. What are graphene field effect transistors (gfets). `https://www.graphenea.com/pages/what-are-graphene-field-effect-transistors-gfets`, Jul 2012.

[5] A. H. Castro Neto, F. Guinea, N. M. Peres, K. S. Novoselov, and A. K. Geim. The electronic properties of graphene. *Reviews of Modern Physics*, 81(1):109–162, 2009.

[6] Chu et al., S.Y.F. The lund/lbnl nuclear data search. `http://nucleardata.nuclear.lu.se/toi/index.asp`, 1999.

[7] Eljen Technology. *General purpose plastic scintillator EJ-200 EJ-204, EJ-208, EJ-212*, 2021.

[8] A. K. Geim and K. S. Novoselov. The rise of graphene. *Nature Materials*, 6(3):183–191, Mar 2007.

[9] A. Ghassemi, K. Sato, and K. Kobayashi. *MPPC Technical Report*. Hamamatsu Photonics K.K., 2017.

[10] A. J. M. Giesbers. Physics in graphene & quantum rings : from mesoscopic device fabrication to measurement in high magnetic fields. 2010.

[11] Graphenea. Gfet-s10 for sensing applications. `https://www.graphenea.com/products/gfet-s10-for-sensing-applications-10-mm-x-10-mm?variant=39420477243550s`, 2020.

[12] Graphenea. *Measurement Protocols and Handling Instructions - Graphene Field-Effect Transistor Chip: S10*, 2020.

[13] Graphenea. *Technical Datasheet - Graphene Field-Effect Transistor Chip: S10*, 2020.

[14] Hamamatsu Photonics K.K. *S13360 series - MPPCs for precision measurement*, August 2016.

[15] Hamamatsu Photonics K.K. *C12332-01 - Simple evaluation starter kit for non-cooled MPPC*, March 2020.

[16] Igor Jovanovic, Edward Cazalas, Isaac Childres, Amol Patil, Ozhan Koybasi, and Yong P. Chen. Graphene field effect transistor-based detectors for detection of ionizing radiation. *2013 3rd International Conference on Advancements in Nuclear Instrumentation, Measurement Methods and their Applications (ANIMMA)*, 2013.

[17] Jia-Ming Liu and I-Tan Lin. *Graphene Photonics*. Cambridge University Press, 2018.

[18] Smets Arno Hendrikus Marie, Jager Klaus, Olindo Isabella, van Swaaij Rene A.C.M.M, and Miro Zeman. *Solar energy: The physics and engineering of photovoltaic conversion, technologies and systems*. UIT Cambridge, 2016.

[19] K. S. Novoselov, A. K. Geim, S. V. Morozov, D. Jiang, Y. Zhang, S. V. Dubonos, I. V. Grigorieva, and A. A. Firsov. Electric field effect in atomically thin carbon films. *Science*, 306(5696):666–669, 2004.

[20] K. S. Novoselov, D. Jiang, F. Schedin, T. J. Booth, V. V. Khotkevich, S. V. Morozov, and A. K. Geim. Two-dimensional atomic crystals. *Proceedings of the National Academy of Sciences*, 102(30):10451–10453, 2005.

[21] N. M. R. Peres. Colloquium: The transport properties of graphene: An introduction, Sep 2010.

[22] F. Schedin et al. Detection of individual gas molecules adsorbed on graphene. *Nature Materials*, 6(9):652–655, 2007.

[23] Haomin Wang, Yihong Wu, Chunxiao Cong, Jingzhi Shang, and Ting Yu. Hysteresis of electronic transport in graphene transistors. *ACS Nano*, 4(12):7221–7228, 2010.

[24] J. Warbinek, D. Leimbach, D. Lu, K. Wendt, D. J. Pegg, A. Yurgens, D. Hanstorp, and J. Welander. A graphene-based neutral particle detector. *Applied Physics Letters*, 114(6):061902, 2019.

[25] U. Kushan Wijewardena, Tharanga Nanayakkara, Rasanga Samaraweera, Sajith Withanage, Annika Kriisa, and Ramesh G. Mani. Effects of long-time current annealing to the hysteresis in cvd graphene on sio2. *MRS Advances*, 4(61-62):3319–3326, 2019.